Korean J. Chem. Eng., **31**(8), 1405-1412 (2014)
DOI: 10.1007/s11814-014-0074-7

pISSN: 0256-1115
eISSN: 1975-7220

Removal of elemental mercury from simulated flue gas by cerium oxide modified attapulgite

Donglei Shi*,, Yu Lu*, Zhe Tang**, Fennv Han**, Ruoyu Chen*, and Qi Xu**,†**

*School of Petrochemical Engineering, Changzhou University, Changzhou 213164, P. R. China
**College of Chemical Engineering and Biological, Yancheng Institute of Technology, Yancheng 224051, P. R. China
(*Received 30 December 2013 • accepted 27 February 2014*)

Abstract−A novel catalyst CeO_2/ATP was developed to remove Hg^0 from coal fired gas. This is new way to use the facile, cheap and larger BET specific surface area catalyst attapulgite (ATP) as support to remove Hg^0 from coal fired gas. The Hg^0 removal and oxidation efficiency of CeO_2/ATP (1 : 1) is up to 97.75% and 92.23% at 200 °C, respectively. We also found that ATP plays an important role in improving the catalyst activity of CeO_2/ATP, which can make CeO_2/ATP have more stable catalyst activity at broader temperature range and obtain lower optimum activity temperature. Other influencing factors, such as temperature and flue gas environment (SO_2, Cl_2, NO), are also investigated in order to get a clear understanding of the experiment. The formation mechanisms are also proposed.

Keywords: Element Mercury, Attapulgite, Cerium Oxide, Catalytic Oxidation, Flue Gas

INTRODUCTION

Mercury emission is an environmental and health problem due to high toxicity, persistence, volatility and long-rang mobility [1-3]. Coal-fired power plants are one of the largest anthropogenic sources of mercury emissions. On March 28, 2013, the U.S. Environmental Protection Agency (EPA) updated emission limits for new power plants under the Mercury and Air Toxics Standards (MATS) [4]. Furthermore, the State Environment Protected Administration of China (SEPA) also published the *Emission Standard of* Air Pollutions for Thermal Power Plants (GB13223-2011), in which the mercury emission limit is 0.03 mg/m^3 [5].

The forms of Hg in coal-fired flue gas include elemental mercury (Hg^0), oxidized mercury (Hg^{2+}) and particle-bound mercury (Hg^p) [6]. Therein, it is relatively easy to remove Hg^p and Hg^{2+} by existing air pollution control devices (APCDs). For example, Hg^p can be removed along with fly ash by electrostatic precipitators (ESPs) and bag dust collector. Hg^{2+} is soluble in water and thus can be captured by the wet flue gas desulfurization devices (WFGDs). Hg^0 is difficult to directly remove by APCDs due to its high volatility and almost insolubility in water [7]. Consequently, the key technology of the mercury removal in flue gas is the Hg^0 emission control.

If Hg^0 could be oxidized to water-soluble Hg^{2+} by catalytic oxidation of catalysts, it would be easy to remove according to the removal technology of Hg^{2+}, which will be significant for the control of mercury emission in coal-fired flue gas. It has reported that many adsorbents modified with metal oxides, such as CeO_2, Mn_2O_3, Fe_2O_3, CuO and V_2O_5, have been extensively researched and showed a promising performance in heterogeneous oxidation of Hg^0, especially at relative low temperature [8-12]. Among the above metal oxides, CeO_2 has high activity and stability on Hg^0 capture and was the common metal oxide to remove the Hg^0 in coal-fired flue gas by oxidation [13-17], owing to CeO_2 having large oxygen storage capacity and unique redox couple Ce^{3+}/Ce^{4+}. In the reaction process, CeO_2 can act as an oxygen reservoir by storing or releasing via the Ce^{4+}/Ce^{3+} redox couple, and it plays a very important role in Hg^0 removal reaction [18]. Owing to rare-earth manganites' specific chemical and physical properties, they have a great potential for environmental applications as catalysts. Europium, cerium, praseodymium, and samarium manganites are very active in oxidation reactions; moreover, cerium manganite is the most feasible for industrial oxidation processes [19]. However, all the oxidation removal catalysts of Hg^0 have one disadvantage in that the catalyst support is not cheap and easy to get, which limits the catalysts' application in industry. Furthermore, all the above researches about oxidation removal of Hg^0 in coal-fired flue gas have demonstrated that the catalyst with high BET specific surface area and pore volume is conducive to removal of Hg^0. Therefore, it is significant work to find a facile and cheap catalyst or catalyst support of Hg^0 removal with high BET specific surface area and pore volume.

Attapulgite (ATP), with an ideal molecular formula of $[Si_8Mg_5O_{20}(OH)_2(H_2O)_4 \cdot 4H_2O]$, is a species of natural hydrous magnesium-aluminum silicate mineral with 1-D fibrillar morphology, which is easy to get in Jiangsu province of China. It has a zeolite-like pore structure and large surface area [20-22]. Therefore, in many researches, ATP has been used as adsorbent, catalyst, adhesive and as catalyst support [23-29]. Cao et al. [30] synthesized ATP/CuO composites by a deposition-precipitation method and demonstrated ATP/CuO catalyst has good activity for CO oxidation at low temperature. Zhao et al. [25,28] prepared silver and copper modified ATP/TiO_2 photocatalysts by a hydrolysis method and found that the catalyst enhanced degradation of methylene blue. Liu et al. [31] prepared ATP/Fe_2O_3 composites by a co-precipitation technique and found that the composite showed enhanced magnetic properties. Zhang et al. [32] obtained ATP/SnO_2-TiO_2 via an in situ sol-gel method and found that the composite improved photocatalytic removal ability of the

†To whom correspondence should be addressed.
E-mail: xqsteve@ycit.cn

methyl orange under ultraviolet radiation. However, there have been few reports about the removal of Hg^0 in coal-fired flue gas using ATP as catalyst or catalyst support.

We used ATP as catalyst support and CeO_2 as modified metal oxide to explore the effect of Hg^0 removal of coal-fired flue gas. To clearly understand the effect of individual composites of coal-fired flue gas on the catalyst (CeO_2/ATP) and removal result of Hg^0, the coal-fired flue gas in the experiment was simulated flue gas according to the main composites and content of real coal-fired flue gas. The netting-shaped cerium oxide modified attapulgite (CeO_2/ATP) catalysts were synthesized by an in situ sol-gel method and evaluated under a simulated flue gas condition using a lab-scale fixed-bed system. On the whole, CeO_2/ATP catalysts were investigated in this study for Hg^0 removal and oxidation efficiency, including the influences of CeO_2 loading, reaction temperature and individual flue gas components.

EXPERIMENTAL

1. Materials

Attapulgite (ATP) was purchased from Jiangsu Dongda Heating and Machinery Manufacturing Co. Ltd. $CeCl_3 \cdot 7H_2O$ was provided by Sinopharm Chemical Reagent Co. Ltd. Methanol was obtained from Shanghai Pilot Chemical Corporation. Ammonia and anhydrous ethanol were supplied by Jiangsu Tongsheng Chemical Reagent Co. Ltd. All the chemicals except attapulgite (ATP) were analytical grade and used as received without further purification.

2. Preparation of Material (Pretreatment of ATP)

20 g of ATP was dispersed in 300 mL of distilled water for 2 h under vigorous magnetic stirring to form a suspension liquid, then 20 mL of hydrochloric (HCl, 37%) was added to the solutions for 12 h under reflux at room temperature. The solvent was filtered out, and the resultant solid was washed with distilled water to pH=7 and free of chloride (tested with $AgNO_3$ solution). The resultant solid was dried at 80 °C to constant weight. For convenience of description, the pretreatment of ATP is designated ATP, the untreatment of ATP is designated Raw-ATP.

3. Synthesis of CeO_2/ATP

CeO_2/ATP composite catalysts were prepared by a method similar to the method used by Gnanam and Rajendran [33]. 0.1 M $CeCl_3 \cdot 7H_2O$ was dissolved in 100 mL methanol under vigorous stirring at room temperature, and a certain amount of ATP was added slowly to the solution with continuous stirring for about 1 h. Then, 10 mL ammonia was added dropwise into the above solution under mechanical stirring for 6 h to obtain lavender gel. Thereafter, the gel was calcined at 400 °C for 2 h in oven and then milled. Finally, the CeO_2/ATP (the mass ratios of CeO_2/ATP were 1 : 1, 1 : 3, 1 : 6 respectively) composite catalysts were obtained after washing the resultant solid by anhydrous ethanol-distilled water (V : V=1 : 1) and drying at 70 °C.

4. Characterization of Catalysts

The phase structure of the catalysts was determined by an X-ray diffractometer (XRD, DX-2700 diffractometer) using Cu Kα radiation over the 2θ range from 10° to 80°. The FT-IR spectra of the samples were characterized on a NEXUS-670 FT-IR spectroscopy (NICOLET) from 4,000 to 400 cm^{-1}. The morphologies of the samples were observed by using QUANTA200 scanning electron microscope (SEM) (FEI Company). The BET surface area was evaluated by N_2 sorption measurement using Micromeritics ASAP 2010 at 77 K. The average pore diameter and pore volume were obtained

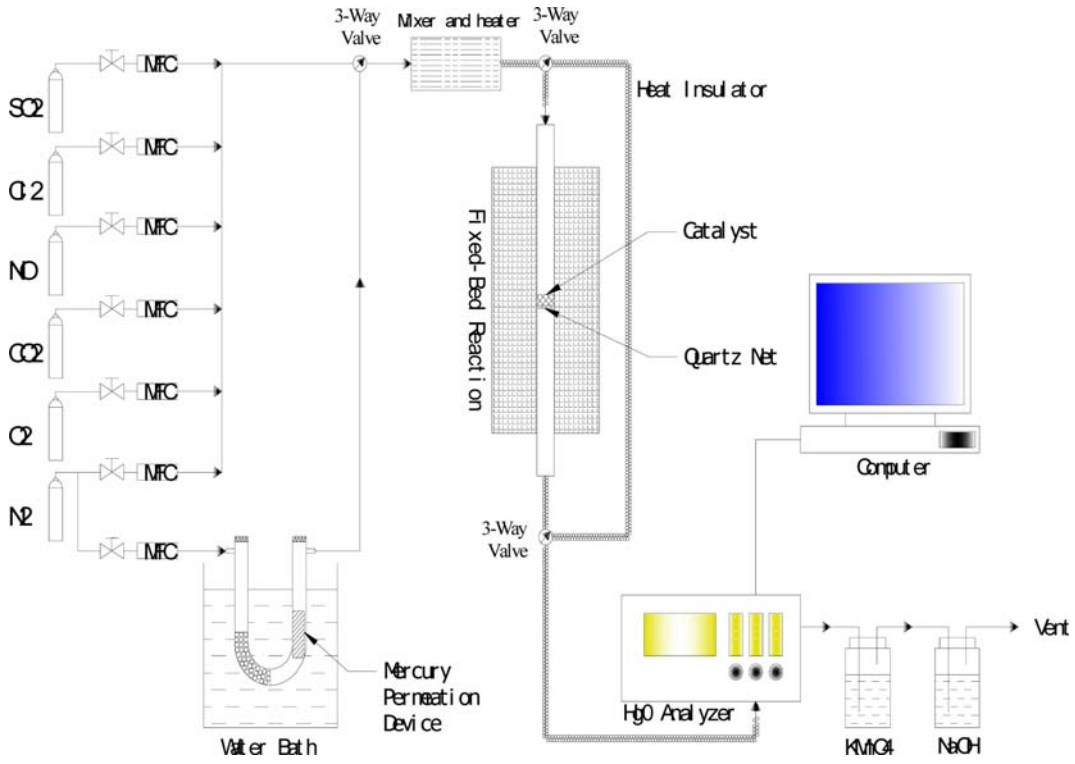

Fig. 1. Schematic diagram of fixed-bed reactor system.

from nitrogen adsorption isotherm.

5. Apparatus and Procedure

Fig. 1 is a schematic diagram of the apparatus used to evaluate Hg^0 removal. The test rig consisted of a simulated flue gas feed system, Hg^0 vapor generating equipment, fixed-bed flow reactor system, and an online mercury analyzer (QM201H China). The simulated flue gas was 6% O_2, 12% CO_2, 300 ppm NO, 1,000 ppm SO_2, 50 ppm Cl_2 and balanced gas N_2. The total flow rate was 1 L/min, which was controlled by mass flow controllers, and the gas hourly space velocity (GHSV) was around 37,700 h^{-1}. The N_2 flow was distributed into two branches: one branch converged with the SO_2, NO, CO_2 and O_2 to form the main gas flow, and the other branch (200 mL/min) passed through the Hg^0 vapor (20 μg/m^3) into the system.

The fixed-bed reactor was composed of a temperature-controllable oven and a quartz tube with an inside diameter of 13 mm. The temperature-controllable oven was occupied to keep the temperature different of fixed-bed reactor within ±2 °C. A fritted quartz disk adsorption bed was placed inside the reactor to prevent the samples from escaping through the bed. After mercury analysis, the exhaust gas should be introduced into the 0.1 M $KMnO_4$ solution before being expelled into the air.

During the experiments, Hg^0 concentration was measured by the mercury analyzer (QM201H China) which can measure merely the concentration of Hg^0. To measure the concentration of total mercury consisting of Hg^0 and oxidized mercury, a 10 wt% stannous chloride ($SnCl_2$) solution was located between the fixed-bed reactor and the analyzer. After passing the $SnCl_2$ solution, the oxidized mercury should be reduced into Hg^0 by $SnCl_2$.

In this study, 0.5 g of the catalyst was used in the experiment from 100 to 260 °C. The Hg^0 oxidation efficiency (E_{oxi}) is calculated as follows:

$$E_{oxi}(\%)=\frac{[Hg]_{total}-[Hg^0]}{[Hg]_{total}}\times 100\% \quad (1)$$

where $[Hg]_{total}$ represents the concentration of total mercury after passing the $SnCl_2$ solution, and $[Hg^0]$ represents the concentration of Hg^0 before passing the $SnCl_2$ solution.

The Hg^0 removal efficiency includes both of mercury adsorption onto the solid and oxidation of elemental mercury. Thus, the Hg^0 removal efficiency (E_{rem}) is defined as follows:

$$E_{rem}(\%)=\frac{[Hg^0]_{in}-[Hg^0]_{out}}{[Hg]_{in}}\times 100\% \quad (2)$$

where $[Hg^0]_{in}$ and $[Hg^0]_{out}$ represent Hg^0 concentration at the inlet and outlet of the fixed-bed reactor.

Furthermore, the Hg^0 adsorption efficiency (E_{ads}) is calculated as follows:

$$E_{ads}(\%)=E_{rem}(\%)-E_{oxi}(\%) \quad (3)$$

RESULTS AND DISCUSSION

1. Catalyst Characteristics

1-1. Structure Characterization

To identify the phase and crystalline structure of CeO_2 on the samples, XRD measurements of ATP (calcined at 400 °C), CeO_2 (calcined at 400 °C), CeO_2/ATP (1 : 1), CeO_2/ATP (1 : 3), CeO_2/ATP (1 : 6) were conducted and the XRD patterns of these samples are shown in Fig. 2. The typical diffraction peaks at 2θ=13.68°, 19.96° and 27.58° exhibited good agreement with the primary diffractions from (200), (040) and (400) planes for ATP. However, the intensity of the three peaks decreased with the increase of CeO_2 and the peak at 2θ=13.68° even disappeared when the loading was above CeO_2/ATP (1 : 6). The typical diffraction peaks at 2θ=28.66°, 33.04°, 47.62° and 56.41° of the CeO_2 can be assigned to (111), (200), (220) and (311) crystalline phase, which could be detected over CeO_2/ATP (1 : 6). Moreover, the intensity of the four peaks increased with the increase of CeO_2, which indicated the CeO_2 crystal particles on the surface of catalysts became bigger. It is noticed that the (111) peak of CeO_2 slightly shifts to higher Bragg angle with the increase of CeO_2, which could indicate that CeO_2 and ATP had interaction in these samples.

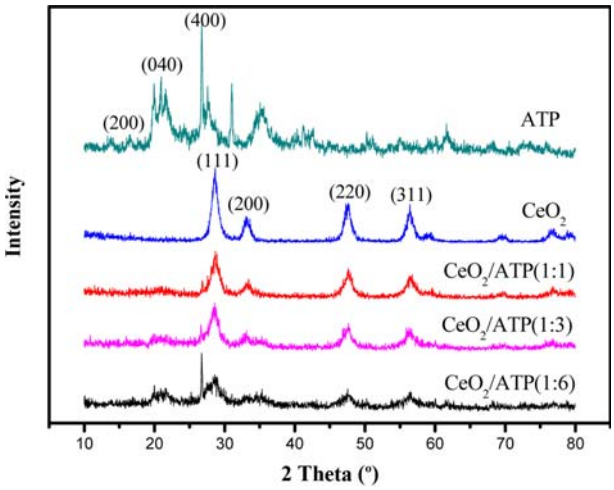

Fig. 2. XRD patterns of ATP, CeO_2, CeO_2/ATP (1 : 1), CeO_2/ATP (1 : 3), CeO_2/ATP (1 : 6).

Fig. 3 shows the FT-IR spectra of ATP (calcined at 400 °C), CeO_2 (calcined at 400 °C), CeO_2/ATP (1 : 1), CeO_2/ATP (1 : 3) and CeO_2/ATP (1 : 6). The band at 1,029.07 cm^{-1} corresponded to Si-O vibra-

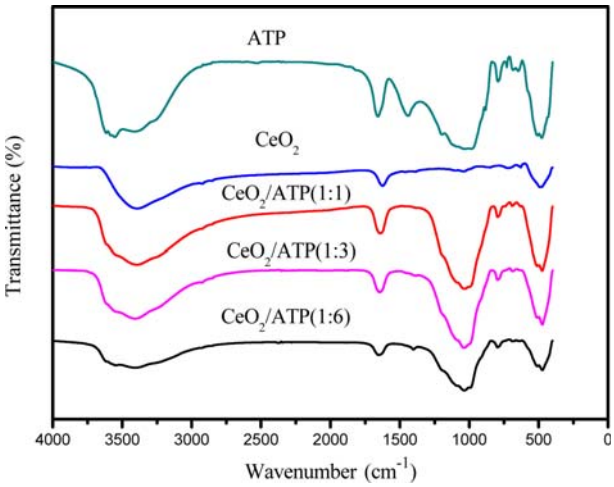

Fig. 3. FT-IR spectra of ATP, CeO_2, CeO_2/ATP (1 : 1), CeO_2/ATP (1 : 3), CeO_2/ATP (1 : 6).

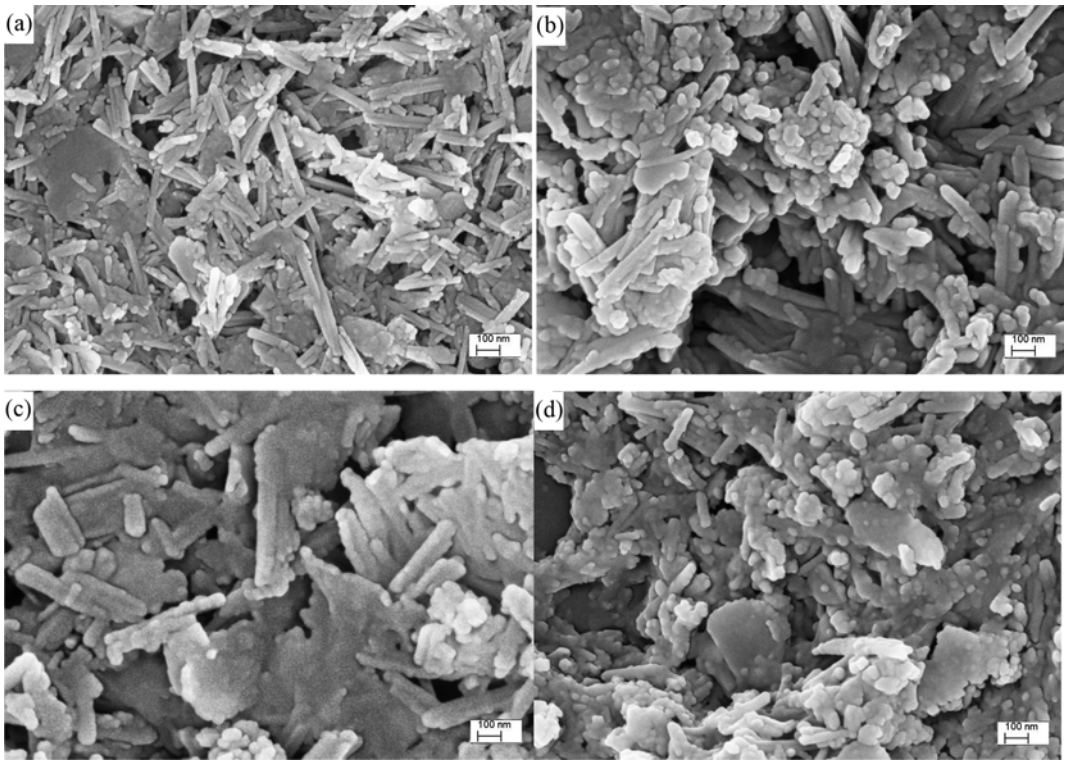

Fig. 4. SEM images of ATP, CeO_2/ATP (1 : 6), CeO_2/ATP (1 : 3) and CeO_2/ATP (1 : 1).

tion mode in ATP. Moreover, two bands at 3,426.73 and 1,633.14 cm^{-1}, respectively, were assigned to the stretching vibration of -OH stretching and bending vibration of water molecules for ATP [34, 35]. Two broad bands of CeO_2 at 624 and 496 cm^{-1} could be detected, which were attributed to the asymmetric stretching mode of Ce-O-Ce bond [36]. However, in the spectra of CeO_2/ATP (1 : 1, 1 : 3, 1 : 6), the characteristic bands of CeO_2 decreased with the increased content of ATP, which implied the presence of rare earth oxides dispersed on the ATP surface in the form of CeO_2, consistent with the analysis in Fig. 2. The FT-IR spectra of CeO_2/ATP (1 : 6) and ATP are almost the same.

1-2. Morphology Characterization

The morphologies and microstructures of the catalysts were examined by SEM. Fig. 4 is the scanning electron micrographs (SEM) of ATP (calcined at 400 ℃) and CeO_2/ATP catalysts. As can be seen in Fig. 4(a), ATP is a fibrous and layered structure and there are large spaces between the layers. However, the fibrous morphology decreases with the increase of CeO_2, and when the amount of CeO_2 is up to 50 wt%, the fibrous morphology almost disappears (Fig. 4(d)). This phenomenon might be due to CeO_2 being widely dispersed on the ATP surface, increasing the active sites of CeO_2 for mercury oxidation, which was beneficial for improving Hg^0 oxidation efficiency in simulated flue gas.

1-3. Textural Property

The nitrogen adsorption-desorption isotherms of Raw-ATP (calcined at 400 ℃), ATP (calcined at 400 ℃), CeO_2 (calcined at 400 ℃), CeO_2/ATP (1 : 1), CeO_2/ATP (1 : 3) and CeO_2/ATP (1 : 6) are shown in Fig. 5. The isotherms of various samples in the Fig. 5 are significantly different, indicating that pore structures of the catalysts are quite different. The isotherms of CeO_2/ATP nanocomposites were

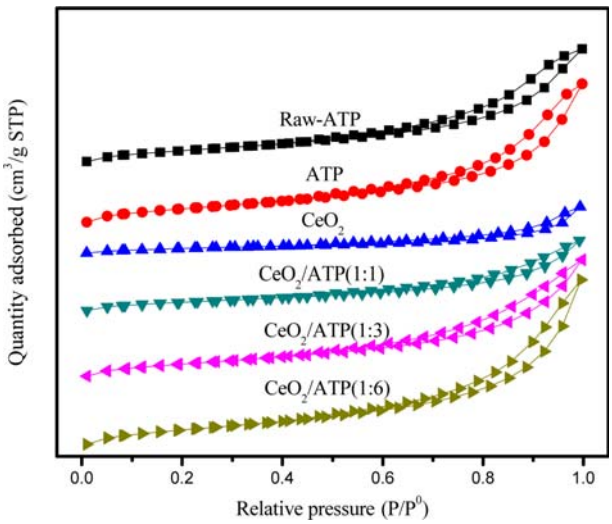

Fig. 5. Nitrogen adsorption-desorption isotherms of Raw-ATP, ATP, CeO_2/ATP (1 : 1), CeO_2/ATP (1 : 3) and CeO_2/ATP (1 : 6).

classified as type IV with clear hysteresis loops from P/P_0=0.45 to 1.0, and the hysteresis loops and the specific surface area became larger and larger following increasing the content of ATP. Moreover, it was observed that the isotherms of CeO_2/ATP (1 : 6) and ATP were almost the same. The ATP adsorption occupied an important position during the Hg^0 removal process. The porous properties of the samples are summarized in Table 1, including the specific surface area, micropore area, total pore volume and average pore diameter. CeO_2/ATP (1 : 6) shows the highest BET surface area (S_{BET}) of 173.10 m^2/g, the highest total pore volume of 0.41 cm^3/g and the

Table 1. Physicochemical Characterization of Raw-ATP, ATP, CeO_2, CeO_2/ATP (1 : 1), CeO_2/ATP (1 : 3) and CeO_2/ATP (1 : 6)

Item	Raw-ATP	ATP	CeO_2	CeO_2/ATP (1 : 1)	CeO_2/ATP (1 : 3)	CeO_2/ATP (1 : 6)
BET surface area (m^2/g)	138.55	165.27	61.84	109.34	149.46	173.10
Micropore area (m^2/g)	18.77	28.31	10.50	22.80	21.87	20.84
Total pore volume (cm^3/g)	0.29	0.36	0.12	0.19	0.30	0.41
Average pore diameter (nm)	8.38	8.58	7.86	6.83	8.00	9.55

longest average pore diameter of 9.55 nm. However, the S_{BET}, the total pore volume and the average pore diameter of ATP decreases to some extent with the increase of CeO_2. Especially, the S_{BET}, the total pore volume and the average pore size for CeO_2/ATP (1 : 1) was reduced to 109.34 m^2/g, 0.91 cm^3/g and 6.83 nm, respectively. The result could indicate that CeO_2, which existed over the external surface of the samples, would deteriorate the thin pore walls and block internal pores with the increase of CeO_2.

2. Effect of ATP

To understand the effect of ATP on the removal and oxidation of Hg^0 in coal-fired flue gas, four catalysts were designed like ATP, Raw-ATP, CeO_2 and CeO_2/ATP (1 : 6). Note that the preparation of CeO_2 is the same as the catalyst CeO_2/ATP (1 : 6), and the amount of CeO_2 used in the experiment is equal to the content of CeO_2 in the catalyst CeO_2/ATP (1 : 6). Fig. 6 is the removal and oxidation of Hg^0 in coal-fired flue gas on the catalyst of ATP, CeO_2 and CeO_2/ATP (1 : 6). It can be seen that the catalyst CeO_2/ATP (1 : 6) has best performance in the three catalysts, which gets the best removal (up to 89.01%) and oxidation (up to 81.99%) of Hg^0 at 200 °C. The result indicates that the catalyst of CeO_2/ATP is feasible for removing the Hg^0 of coal-fired flue gas, and most of Hg^0 is removed by the catalyst CeO_2/ATP. Furthermore, the variation trend of Hg^0 removal or oxidation under the catalyst of ATP is very similar to the variation trend of the CeO_2/ATP (1 : 6). Both of them have the same optimum activity temperature at 200 °C. Below the temperature, the Hg^0 removal or oxidation increases with the increase of temperature. Beyond the temperature, the Hg^0 removal or oxidation decreases with the increase of temperature. However, the difference of Hg^0 removal or oxidation between the two catalysts is higher beyond the optimum activity temperature and is less approached at the optimum activity temperature. The Hg^0 removal is 67.0% at 100 °C, 65.63% at 260 °C, 89.01% at 200 °C in the catalyst of CeO_2/ATP (1 : 6). While, the Hg^0 removal in the catalyst of ATP is 32.05% at 100 °C, 28.80% at 260 °C, 74.13% at 200 °C. Moreover, the variation trend of Hg^0 removal or oxidation under the catalyst of CeO_2 is different from that of the former two catalysts, which have poor performance at low temperature. From 100 °C to 180 °C, the best Hg^0 removal is only 27.19% at 140 °C. Furthermore, the optimum activity of the CeO_2 is 220 °C, which is higher than that of CeO_2/ATP (1 : 6) and ATP. It means that after CeO_2 is incorporated ATP, ATP can make the catalyst have the lower temperature activity and stronger stability of Hg^0 removal or oxidation, especially at low temperature (<180 °C). The reason may be due to the larger specific surface area and pore volume. The supposition is supported by the result of adsorption, which can be seen in Table S1 (shown in Supplementary Material). The average Hg^0 adsorption under the catalyst of CeO_2 is only 2.0%. While, the average Hg^0 adsorptions under CeO_2/ATP (1 : 6) and ATP are up to 8.0% and 12.0%, respectively. From the Table 1, BET specific surface areas of CeO_2, CeO_2/ATP (1 : 6), and ATP are 61.84, 165.27 and 173.10 m^2/g. After CeO_2 is loaded on the ATP, ATP acts as a support to make the CeO_2 disperse uniformly and inhibit aggregation of CeO_2. Therefore, after CeO_2 is loaded on the ATP, the catalyst has more CeO_2 activity.

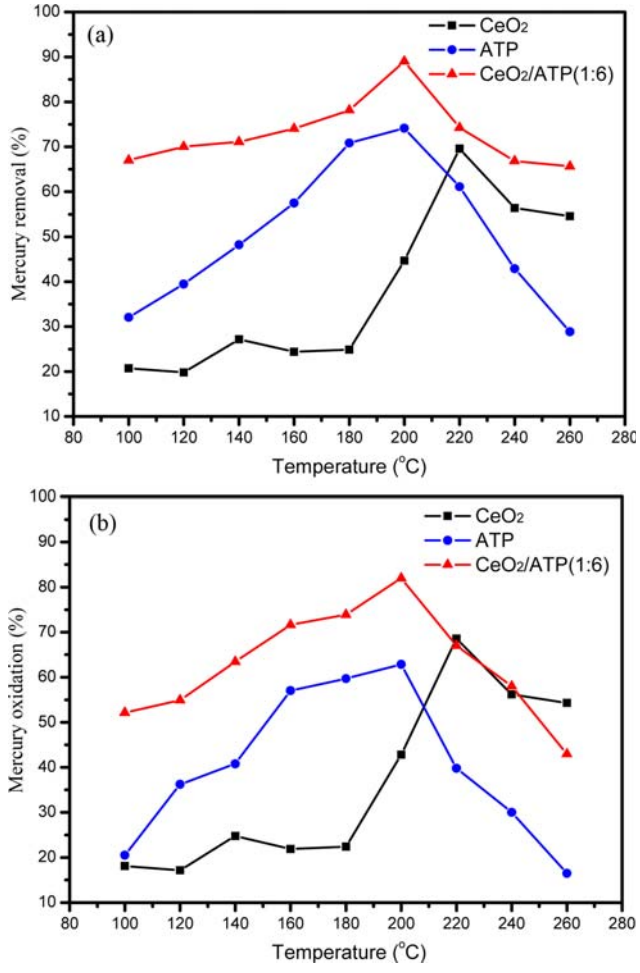

Fig. 6. The removal (a) and oxidation efficiency (b) of Hg^0 on the catalysts CeO_2, ATP, and CeO_2/ATP (1 : 6).

To understand the texture property of ATP on the Hg^0 removal and oxidation, Raw-ATP and ATP, which have different specific surface area and pore volume, were used in the experiment. ATP is the product of treatment of Raw-ATP in HCl solution under hydrothermal method. Normally, ATP should be have a larger BET specific surface area and pore volume than that of Raw-ATP. From Table 1, BET specific surface area and pore volume are 138.55 m^2/g and 8.38 cm^3/g for Raw-ATP, while, 165.27 m^2/g and 8.58 cm^3/g for ATP. The performance of Hg^0 removal and oxidation under these

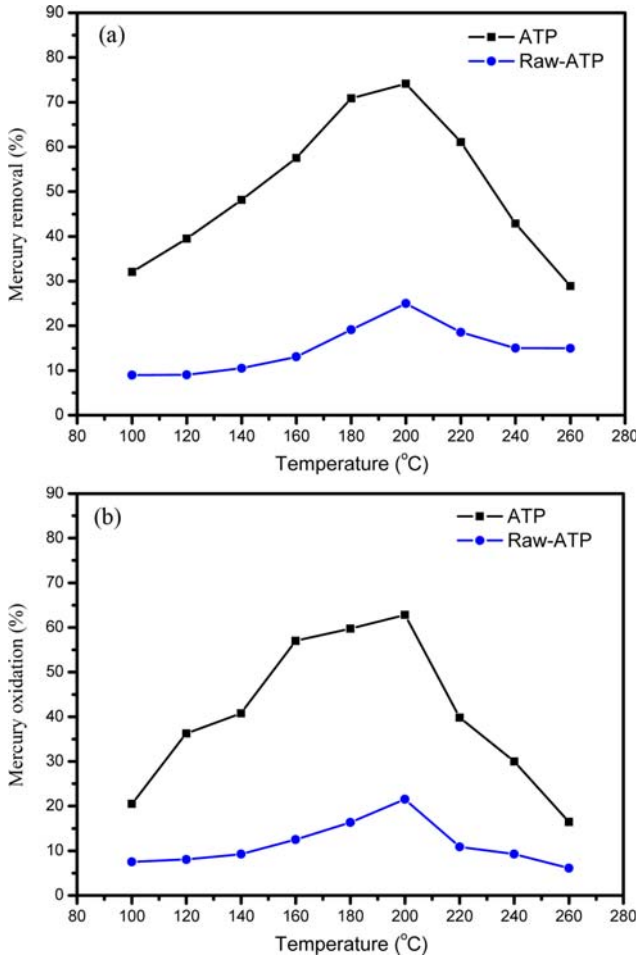

Fig. 7. Hg^0 removal (a) and oxidation (b) under the catalyst of ATP and Raw-ATP.

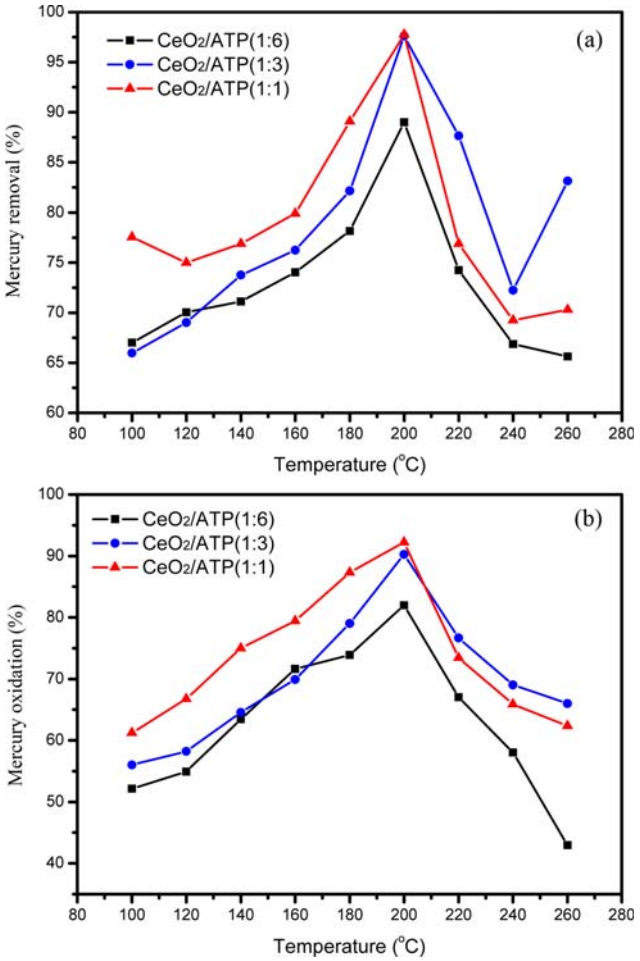

Fig. 8. Hg^0 removal (a) and oxidation (b) under the catalyst of CeO_2/ATP (1 : 6), CeO_2/ATP (1 : 3) and CeO_2/ATP (1 : 1).

two catalysts is shown in Fig. 7. ATP has better efficiency of Hg^0 removal and oxidation than that of Raw-ATP. At optimum activity temperature of 200 °C, the Hg^0 removal and oxidation efficiency under ATP are up to 74.13% and 62.85%. While, at the same optimum activity temperature of 200 °C, the Hg^0 removal and oxidation efficiency under Raw-ATP are only to 25.01% and 21.07%. Furthermore, it can be seen in Table S1 that the average adsorptions of Hg^0 of ATP and Raw-ATP are 12.0% and 4.0%. So the catalyst with larger BET specific surface area and pore volume has better efficiency of Hg^0 removal and oxidation. Moreover, a little residual HCl in ATP can enhance the oxidation of Hg^0, because HCl was not washed clean in the experimental part [16].

3. Effect of CeO_2

To understand the effect of CeO_2 on the removal and oxidation of Hg^0 in coal-fired flue gas, three catalysts were designed like CeO_2/ATP (1 : 1), CeO_2/ATP (1 : 3) and CeO_2/ATP (1 : 6). Hg^0 removal and oxidation efficiency on CeO_2/ATP (1 : 1), CeO_2/ATP (1 : 3) and CeO_2/ATP (1 : 6) at various temperatures are shown in Fig. 8. It is evident that the E_{rem} and E_{oxi} are improved with the increase of CeO_2. The removal and oxidation efficiency for CeO_2/ATP (1 : 1) is up to 97.75% and 92.23% at 200 °C, respectively. The performance was close to or better than other reports [13,16]. However, the removal and oxidation efficiency of CeO_2/ATP (1 : 3) is 97.61% and 90.23%, respectively, which is very close to CeO_2/ATP (1 : 1). This means that further increasing the content of CeO_2 after CeO_2/ATP (1 : 1) will not improve the removal and oxidation of Hg^0 by much. The Hg^0 oxidation capacity of CeO_2 is ascribed to its large oxygen storage capacity and unique redox couple Ce^{3+}/Ce^{4+} [13-15].

4. Effect of SO_2, Cl_2 and NO on Hg^0 Removal and Oxidation

To better understand Hg^0 removal and oxidation capacity over CeO_2/ATP (1 : 1), it is necessary to explore the roles of individual flue gas components on Hg^0 removal and oxidation efficiencies, especially SO_2, Cl_2 and NO. Experiments were conducted at the optimal temperature of 200 °C by mixing Hg^0 with individual flue components in combination with 6% O_2, balanced with N_2, and the experimental result are shown in Fig. 9.

4-1. Effect of SO_2

To study the mercury performance of CeO_2/ATP catalysts in the presence of SO_2, four different concentrations of SO_2 (0 ppm, 500 ppm, 1,000 ppm and 1,500 ppm) were used for the removal of Hg^0 over CeO_2/ATP (1 : 1) catalyst. Fig. 9(a) shows that E_{rem} and E_{oxi} increased when the concentration of SO_2 was less than 1,000 ppm. This result is attributed to the fact that in the presence of gas phase O_2, SO_2 could be oxidized by chemisorbed oxygen to form SO_3 [8]. And the produced SO_3 constituted new chemisorption sites for Hg^0 and could react with Hg^0 to produce $HgSO_4$ [14]. The two redox

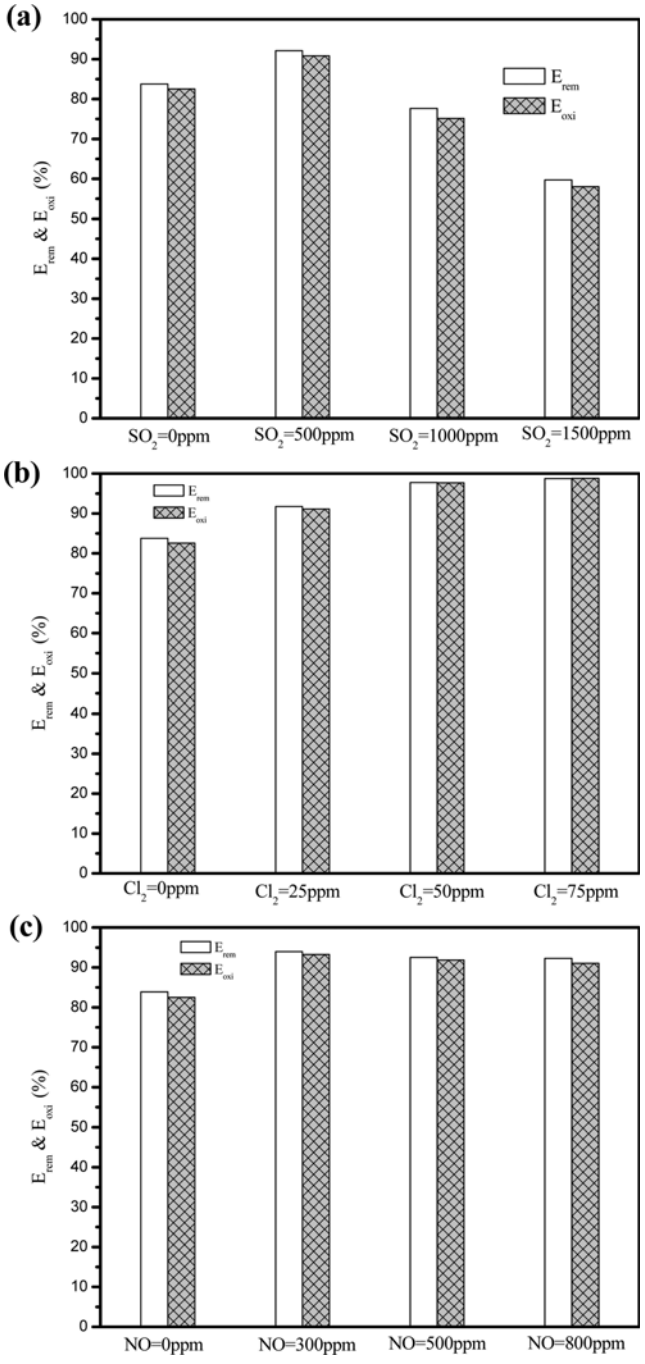

Fig. 9. Effect of individual flue gas components on Hg^0 removal and oxidation efficiency of CeO_2/ATP (1 : 1).

reactions were proposed as follows:

$$SO_2 + 1/2O_2 \xrightarrow{Catalyst} SO_3 \quad (4)$$

$$Hg^0 + SO_3 + 1/2O_2 \xrightarrow{Catalyst} HgSO_4 \quad (5)$$

However, the E_{rem} and E_{oxi} decreased when the concentration of SO_2 was increased to 1,500 ppm. The decrease of E_{oxi} could be due to the competition of Hg^0 and SO_2 to similar active sites on the catalyst surface [8].

4-2. Effect of Cl_2

The main oxidized Hg in coal-fired flue gas exists in the form of $HgCl_2$ [37]; thus Cl_2 is the most important composition of flue gas for Hg^0 oxidation. To identify the effect of Cl_2 for the mercury removal in simulated flue gas, four different concentrations of Cl_2 (0 ppm, 25 ppm, 50 ppm and 75 ppm) were selected in the mercury removal experiments. Fig. 9(b) shows that E_{rem} and E_{oxi} increased constantly with increase of Cl_2 concentration, improved to about 98.75% and 98.62% in the presence of Cl_2 at 75 ppm. It is evident that the existence of gas phase O_2 could supply the consumption of lattice oxygen. The high oxygen concentration on the surface of the catalysts could promote the Cl_2 into Cl^*. Hg^0 would react with Cl^* to form HgCl, and the produced HgCl could react with the other Cl^* to produce $HgCl_2$. The two redox reactions could be speculated as follows:

$$Cl^* + Hg^0 \rightarrow HgCl \quad (6)$$

$$HgCl + Cl^* \rightarrow HgCl_2 \quad (7)$$

4-3. Effect of NO

To understand the effect of NO for the mercury removal in simulated flue gas, four different concentrations of NO (0 ppm, 300 ppm, 500 ppm and 800 ppm) were used for the removal of Hg^0 by CeO_2/ATP (1 : 1) catalyst. As illustrated in Fig. 9(c), 300 ppm NO resulted in 94.01% of mercury removal and 93.24% of mercury oxidation. It has been revealed that Ce^{3+} on the catalyst surface could promote the oxidation of NO into NO_2, and NO_2 was demonstrated to significantly improve heterogeneous oxidation of Hg^0 on fly ash and on activated carbon based sorbents [38,39]. However, E_{rem} and E_{oxi} did not change substantially when the NO concentration increased to 500 ppm and 800 ppm. It could be because the oxygen stored on the CeO_2/ATP (1 : 1) catalyst was sufficient for Hg^0 oxidation. The higher E_{oxi} was obtained, indicating that NO participated in the Hg^0 oxidation reaction and volatile mercuric compounds, like $Hg(NO_3)_2$, were generated. The specific reaction pathway could be summarized as follows:

$$NO + 1/2O_2 \xrightarrow{Catalyst} NO_2 \quad (8)$$

$$Hg^0 + NO_2 \rightarrow HgO + NO \quad (9)$$

$$Hg^0 + 2NO_2 + O_2 \rightarrow Hg(NO_3)_2 \quad (10)$$

CONCLUSIONS

CeO_2/ATP catalysts prepared by the sol-gel method were investigated for their ability to remove and oxidize Hg^0 in a lab-scale fixed-bed system. Results showed that the Hg^0 removal and oxidation efficiency of CeO_2/ATP catalysts was higher than ATP and improved with the increase of CeO_2 under the simulated flue gas condition. Moreover, Hg^0 removal and oxidation efficiency first increased and then decreased with increasing temperature from 100 to 260 °C, and the optimal temperature was 200 °C. It was beneficial for the mercury removal and oxidation using CeO_2/ATP (1 : 1) catalyst in the presence of O_2 when SO_2 was added into the simulated flue gas. But a high SO_2 concentration (1,000 ppm) was not conducive for elemental mercury removal and oxidation. The optimal concentration was 500 ppm. Both Cl_2 and NO promoted Hg^0 removal and oxidation ability of CeO_2/ATP (1 : 1), especially in the presence of Cl_2. When Cl_2 (50 ppm and 75 ppm) and NO (300 ppm, 500 ppm and 800 ppm) were added, the Hg^0 removal and oxidation effi-

ciency was higher than 95% and 90%, respectively. In summary, CeO_2/ATP catalysts were feasible for Hg^0 oxidation in flue gas. Future work should be conducted under the simulated flue gas condition to investigate the reaction mechanism of Hg^0 oxidation on CeO_2/ATP catalysts.

ACKNOWLEDGEMENTS

This work was supported financially by the Innovation Fund Project of Yancheng Institute of Technology (YKB201106) and the Open Fund Project of Environmental Protection Department of Jiangsu Province (2012019).

REFERENCES

1. United Nations Environment Programme (UNEP), Global Mercury Assessment, UNEP Chemicals, Geneva, Switzerland, December, 2002.
2. J. H. Pavlish, E. A. Sondreal, M. D. Mann, E. S. Olson, K. C. Galbreath, D. L. Laudal and S. A. Benson, *Fuel Process. Technol.*, **82**, 89 (2003).
3. A. A. Presto and E. J. Granite, *Environ. Sci. Technol.*, **40**, 5601 (2006).
4. U.S. Environmental Protection Agency, Mercury and Air Toxics Standards (MATS), http://www.epa.gov/airquality/powerplanttoxics/actions.html, Accessed on 24.02.14.
5. State Environmental Protection Administration of China (SEPA), *Emission standard of air pollution for thermal power plants*, GB 13223-2011, SEPA, Beijing (2011).
6. K. C. Galbreath and C. J. Zygarlicke, *Fuel Process. Technol.*, **65**, 289 (2000).
7. Z. Qu, N. Q. Yan, P. Liu, J. P. Jia and S. J. Yang, *J. Hazard. Mater.*, **183**, 132 (2010).
8. H. L. Li, C. Y. Wu, Y. Li, L. Q. Li, Y. C. Zhao and J. Y. Zhang, *Chem. Eng. J.*, **219**, 319 (2013).
9. L. Li, P. M. Sreekanth, P. G. Smimiotis, S. W. Thiel and N. G. Pinto, *Energy Fuels*, **22**, 2299 (2008).
10. F. H. Kong, J. R. Qiu, H. Liu, R. Zhao and Z. H. Ai, *J. Environ. Sci.*, **23**, 699 (2011).
11. A. Yamaguchi, H. Akiho and S. Ito, *Powder Technol.*, **180**, 222 (2008).
12. S. He, J. S. Zhou, Y. Q. Zhu, Z. Y. Luo, M. J. Ni and K. F. Cen, *Energy Fuels*, **23**, 253 (2009).
13. L. H. Tian, C. T. Li, Q. Li, G. M. Zeng, Z. Gao, S. H. Li and X. P. Fan, *Fuel*, **88**, 1687 (2009).
14. X. P. Fan, C. T. Li, G. M. Zeng, Z. Gao, L. Chen, W. Zhang and H. L. Gao, *Energy Fuels*, **24**, 4250 (2010).
15. X. Wen, C. Li, X. Fan, H. Gao, W. Zhang, L. Chen, G. Zeng and Y. Zhao, *Energy Fuels*, **25**, 2939 (2011).
16. W. H. Hou, J. S. Zhou, P. Qi, X. Gao and Z. Y. Luo, *Chem. Eng. J.*, **241**, 131 (2014).
17. H. L. Li, C. Y. Wu, L. Q. Li, Y. Li, Y. C. Zhao and J. Y. Zhang, *Fuel*, **113**, 726 (2013).
18. Q. Wan, L. Duan, K. B. He and J. H. Li, *Chem. Eng. J.*, **170**, 512 (2011).
19. D. Alami, *Environ. Eng. Res.*, **18**, 211 (2013).
20. J. L. Cao, G. S. Shao, Y. Wang, Y. P. Liu and Z. Y. Yuan, *Catal. Commun.*, **9**, 2555 (2008).
21. M. S. Barrios, L. V. F. González, M. A. V. Rodríguez and J. M. M. Pozas, *Appl. Clay Sci.*, **10**, 247 (1995).
22. Z. G. Chen, F. Chen, X. Z. Li, X. W. Lu, C. Y. Ni and X. B. Zhao, *J. Rare Earths*, **28**, 566 (2010).
23. H. Chen and A. Q. Wang, *J. Colloid Interface Sci.*, **307**, 309 (2007).
24. J. H. Huang, Y. F. Liu, Y. Liu and X. G. Wang, *J. Amer. Oil Chem. Soc.*, **84**, 687 (2007).
25. D. F. Zhao, J. Zhou and N. Liu, *Mater. Charact.*, **58**, 249 (2007).
26. D. M. A. Melo, J. A. C. Ruiz, M. A. F. Melo, E. V. Sobrinho and A. E. Martinelli, *J. Alloy Compd.*, **344**, 352 (2002).
27. S. D. Miao, Z. M. Liu, Z. F. Zhang, B. X. Han, Z. J. Miao, K. L. Ding and G. M. An, *J. Phys. Chem. C*, **111**, 2185 (2007).
28. D. F. Zhao, J. Zhou and N. Liu, *Mater. Sci. Eng A*, **431**, 256 (2006).
29. D. M. A. Melo, J. A. C. Ruiz, M. A. F. Melo, E. V. Sobrinho and M. Schmall, *Micropor. Mesopor. Mater.*, **38**, 345 (2000).
30. J. L. Cao, G. S. Shao, Y. Wang, Y. P. Liu and Z. Y. Yuan, *Catal. Commun.*, **9**, 2555 (2008).
31. Y. S. Liu, P. Liu, Z. X. Su, F. S. Li and F. S. Wen, *Appl. Surf. Sci.*, **255**, 2020 (2008).
32. L. L. Zhang, F. J. Lv, W. G. Zhang, R. Q. Li, H. Zhong, Y. J. Zhao, Y. Zhang and X. J. Wang, *J. Hazard. Mater.*, **171**, 294 (2009).
33. S. Gnanam and V. Rajendran, *J. Sol-Gel Sci. Technol.*, **58**, 62 (2011).
34. X. Z. Li, C. Y. Ni, C. Yao and Z. G. Chen, *Appl. Catal. B: Environ.*, **117**, 118 (2012).
35. G. Zhang, Z. L. He and W. Xu, *Chem. Eng. J.*, **183**, 315 (2012).
36. D. S. Zhang, H. X. Fu, L. Y. Shi, C. S. Pan, Q. Li, Y. L. Chu and W. J. Yu, *Inorg. Chem.*, **46**, 2446 (2007).
37. H. L. Li, Y. Li, C. Y. Wu and J. Y. Zhang, *Chem. Eng. J.*, **169**, 186 (2011).
38. G. A. Norton, H. Q. Yang, R. C. Brown and D. L. Laudal, *Fuel*, **82**, 107 (2003).
39. S. J. Miller, G. E. Dunham, E. S. Olson and T. D. Brown, *Fuel Process. Technol.*, **65**, 343 (2000).

Supporting Information

Removal of elemental mercury from simulated flue gas by cerium oxide modified attapulgite

Donglei Shi*,*, Yu Lu*, Zhe Tang**, Fennv Han**, Ruoyu Chen*, and Qi Xu**,†**

*School of Petrochemical Engineering, Changzhou University, Changzhou 213164, P. R. China
**College of Chemical Engineering and Biological, Yancheng Institute of Technology, Yancheng 224051, P. R. China
(*Received 30 December 2013 • accepted 27 February 2014*)

Table S1. Hg^0 removal, oxidation and adsorption efficiency under the catalyst of CeO_2, Raw-ATP, ATP, CeO_2/ATP (1 : 6), CeO_2/ATP (1 : 3) and CeO_2/ATP (1 : 1) at various temperatures in our work

Samples	Temperature (°C)	E_{rem} (%)	E_{oxi} (%)	E_{ads} (%)
CeO_2	100	20.74	18.1	2.64
	120	19.82	17.14	2.68
	140	27.19	24.76	2.43
	160	24.42	21.9	2.52
	180	24.88	22.38	2.5
	200	44.7	42.86	1.84
	220	69.59	68.57	1.02
	240	56.38	56.19	0.19
	260	54.53	54.29	0.24
Raw-ATP	100	9.01	7.5	1.51
	120	9.03	8.03	1
	140	10.5	9.26	1.24
	160	13.1	12.51	0.59
	180	19.1	16.33	2.77
	200	25.01	21.52	3.49
	220	18.57	10.87	7.7
	240	15.01	9.27	5.74
	260	14.95	6.1	8.85
ATP	100	32.05	20.49	11.56
	120	39.5	36.23	3.27
	140	48.2	40.78	7.42
	160	57.52	57.03	0.49
	180	70.86	59.72	11.14
	200	74.13	62.85	11.28
	220	61.12	39.81	21.31
	240	42.87	30.02	12.85
	260	28.88	16.45	12.43

Table S1. Continued

Samples	Temperature (°C)	E_{rem} (%)	E_{oxi} (%)	E_{ads} (%)
CeO_2/ATP (1 : 6)	100	67.01	52.16	14.85
	120	70.03	54.91	15.12
	140	71.11	63.45	7.66
	160	74.03	71.63	2.4
	180	78.15	73.89	4.26
	200	89.01	81.99	7.02
	220	74.25	67.01	7.24
	240	66.87	58.03	8.84
	260	65.63	42.96	22.67
CeO_2/ATP (1 : 3)	100	65.97	56.01	9.96
	120	69.02	58.22	10.8
	140	73.76	64.55	9.21
	160	76.23	69.92	6.31
	180	82.17	79.01	3.16
	200	97.61	90.23	7.38
	220	87.65	76.67	10.98
	240	72.24	69.02	3.22
	260	83.15	66.01	17.14
CeO_2/ATP (1 : 1)	100	77.53	61.23	16.3
	120	75	66.75	8.25
	140	76.89	75.01	1.88
	160	79.9	79.45	0.45
	180	89.1	87.31	1.79
	200	97.75	92.23	5.52
	220	76.89	73.45	3.44
	240	69.25	65.87	3.38
	260	70.3	62.35	7.95